Available online at www.sciencedirect.com
ScienceDirect
Journal of Sound and Vibration 299 (2007) 247–260
JOURNAL OF SOUND AND VIBRATION
www.elsevier.com/locate/jsvi

Hybrid vibration absorber with virtual passive devices

Shang-Teh Wu*, Yea-Ying Chiu, Yuan-Chih Yeh

Department of Mechanical Engineering, National Yunlin University of Science and Technology, Touliu, Yunlin 640, Taiwan

Received 18 March 2006; received in revised form 5 July 2006; accepted 21 July 2006
Available online 15 September 2006

Abstract

A vibration control scheme integrating a passive mass–spring resonator and a linear actuator is developed. A control algorithm is devised to convert the actuator into an additional set of virtual mass–spring structure of programmable characteristic frequency. The relative motion between the primary body and the reaction mass is measured, as well as the acceleration of the reaction mass. This hybrid dynamic vibration absorber is capable of neutralizing a harmonic disturbance regardless of the detailed dynamics of the primary structure and other passive elements. Stability analysis leads to a simple, explicit stability criterion. Distribution of the counter-disturbance force between the active and passive devices is analyzed, and the transient performance is also investigated. Real-time experiments as well as numerical simulations are conducted to confirm the effectiveness of the proposed scheme.

1. Introduction

This paper presents a novel vibration control method combining a passive resonator and a linear actuator. In parallel to a mechanical spring, the linear actuator acts on the primary body against a reaction mass. Thanks to the active device, characteristic frequency of the hybrid dynamic vibration absorber (hybrid DVA) is tunable by software and the transient performance can be improved. On the other hand, the passive spring helps share the counter-disturbance effort so that the actuator's size and the consumed power can be minimized.

Such a hybrid vibration absorber has been an active research topic. Earlier control methods for the active device include classical full-state feedback controls and fuzzy logic and neural networks (see Ref. [1] for a review). A delayed resonator using a time-delayed position feedback is presented in Ref. [2]. In Ref. [3], the delayed resonator and a PD control are compared experimentally, both measuring relative motions between the reaction mass and the primary body. In Ref. [4] a procedure for pole/zero placement is developed also measuring feedback at coupling point. A band-pass absorber that widens the absorption range is proposed [5] using a band-stop-filter transfer function. In Ref. [6] a notch filter is adopted in an output feedback control. For implementation various types of actuators have been investigated, including linear motors with air springs [7], electromagnetic actuators [3], piezoceramic inertial actuators [8], electrohydraulic actuators [9] and linear

*Corresponding author. Tel.: +886 5 5342601 4111; fax: +886 5 5312062.
E-mail address: wust@yuntech.edu.tw (S.-T. Wu).

0022-460X/$ - see front matter © 2006 Elsevier Ltd. All rights reserved.
doi:10.1016/j.jsv.2006.07.010

voice-coil motors [6]. In Ref. [10] a two reaction-mass resonator is proposed and is shown to be more efficient than the one reaction-mass device in terms of control efforts. Besides the original purpose of neutralizing a harmonic disturbance, the hybrid vibration control technique has also been applied to vibration isolations [9,11,12], and active vehicle suspensions [13].

In this paper a control algorithm emulating the dynamics of a spring–mass mechanism is devised. The virtual passive device acts as an ideal DVA of which the characteristic frequency can be adjusted by tuning the control gains. Compared to the existing control techniques, the proposed scheme directly mimics a DVA *independent of* the passive elements. In other words, it is capable of neutralizing a harmonic disturbance regardless of the detailed dynamics of the primary structure and the parameters of the passive devices (springs and/or dampers) connecting the reaction mass and the primary body. The overall system can be visualized by an equivalent mechanical structure consisting of passive and virtual passive elements and a state-dependent force. Such a method resembles the virtual passive approach in Refs. [14,15], where the actuators are held to an inertial frame rather than acting against a free-moving reaction mass. This "free-ended" configuration has the merits of eliminating vibrations on the spot without transferring the oscillations to the surroundings through the ground base. Unlike the ground-based systems in Refs. [14,15], however, stability is a nontrivial issue for this free-ended scheme because of interactions between the active device and the passive resonator. An explicit stability criterion will be derived in this paper.

The rest of the paper is arranged as follows. Section 2 describes the system under consideration. Section 3 presents the physically motivated control algorithm. It is shown how to visualize the closed-loop system as an equivalent mechanical structure. Stability analysis is conducted in Section 4, where a simple, closed-form stability condition is derived with a physical interpretation. Section 5 analyzes the distribution of counter-disturbance force between the passive and active elements, and investigates the transient performance. Numerical simulations are also conducted in this section. Finally experimental results are presented in Section 5 followed by a conclusion.

2. System description

Fig. 1 shows a conventional DVA for a flexible structure subjected to a harmonic disturbance. The vibration absorber includes a mass–spring pair with a characteristic frequency close to that of the disturbance. It contains an additional damper that helps avoid resonance at other frequencies and raise the effective bandwidth of operations. The damper is essential when the original structure is lightly damped. However, the damper also makes it impossible to achieve complete neutralization of a persistent, harmonic disturbance.

Fig. 2 is a sketch of the hybrid DVA under consideration. It contains a linear actuator embedded in the reaction mass in parallel to the mechanical spring and damper. The linear actuator will be programmed to emulate an additional combination of mechanical spring, damper, and mass via a control law. The feedback signals are the relative displacement and velocity between the primary body and the reaction mass, and the

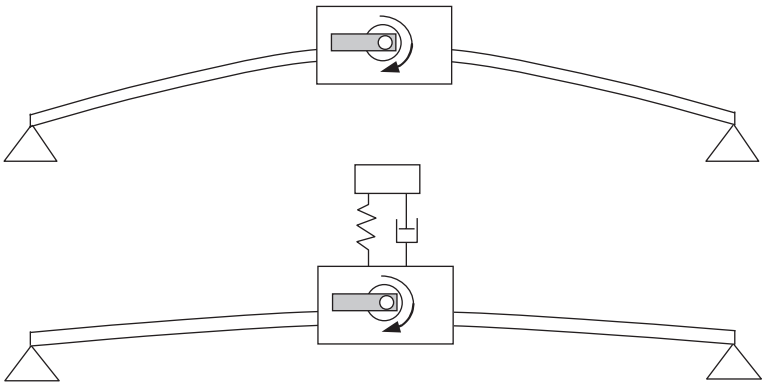

Fig. 1. A structure subjected to cyclic disturbances (up) and one equipped with a dynamic vibration absorber (down).

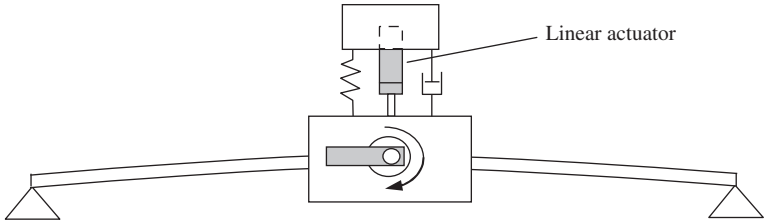

Fig. 2. Hybrid dynamic vibration absorber.

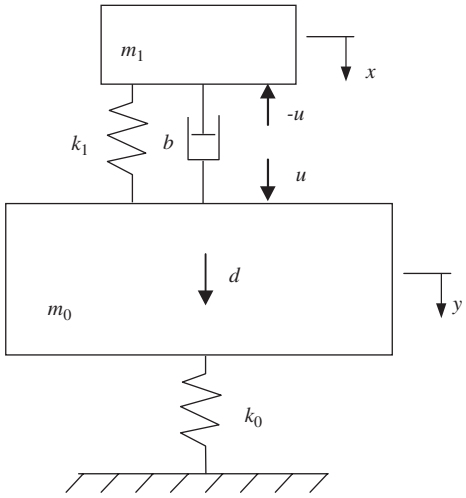

Fig. 3. Simplified model of the control plant.

acceleration of the reaction mass. The sensors include a linear variable differential transformer (LVDT) installed on the linear actuator and an accelerometer glued to the reaction mass. In implementation the relative velocity can be approximated by numerically differentiating the displacement measured by the LVDT.

By simplifying the flexible plate to a mass–spring structure, the system with the hybrid vibration-control mechanism can be modeled as in Fig. 3. The governing equations are

$$m_0\ddot{y} + k_0 y + k_1(y - x) + b(\dot{y} - \dot{x}) = u + d, \tag{1}$$

$$m_1\ddot{x} + k_1(x - y) + b(\dot{x} - \dot{y}) = -u, \tag{2}$$

$$d = a\sin(\omega_0 t + \phi), \tag{3}$$

where y is the displacement of the primary body, x is the displacement of the reaction mass, m_0 and m_1 are respectively the inertia of the primary body and the inertia of the reaction mass, k_0 and k_1 are the spring constants, b is the damping coefficient, u is the control force exerted by the linear actuator, and d is the external disturbing force of radian frequency ω_0. The phase ϕ and amplitude a of the disturbance are uncertain constants.

3. Feedback control and the equivalent system

The control law is devised to be

$$u = k_a(\tilde{z} - \tilde{y}) - b_a\dot{\tilde{y}} + \hat{k}_1\tilde{y}, \tag{4}$$

$$m_a\ddot{\tilde{z}} = -k_a(\tilde{z} - \tilde{y}) - m_a\ddot{x}, \tag{5}$$

where

$$\tilde{y} = y - x. \tag{6}$$

All parameters in Eqs. (4) and (5) are constants with

$$k_a > 0, \quad m_a > 0, \quad b_a + b > 0, \quad k_1 - \hat{k}_1 > 0, \tag{7}$$

and

$$\frac{k_a}{m_a} = \omega_0^2. \tag{8}$$

Note that $\tilde{y}$ is the displacement of the primary body relative to the reaction mass and is measurable by the LVDT. The acceleration $\ddot{x}$ is measured by the accelerometer glued to the reaction mass, and the variable $\tilde{z}$ will be calculated and updated in the controller.

To explore the physical implication of the control law of Eqs. (4) and (5), we define $z = \tilde{z} + \ddot{x}$, or

$$\tilde{z} = z - \ddot{x}. \tag{9}$$

Substitution of Eqs. (6) and (9) into Eqs. (4) and (5) yields

$$u = k_a(z - y) - b_a(\dot{y} - \dot{x}) + \hat{k}_1(y - x), \tag{10}$$

$$m_a\ddot{z} = k_a(y - z). \tag{11}$$

Substitution of Eqs. (10) and (11) back into Eqs. (1) and (2) leads to

$$m_0\ddot{y} + k_0 y + \tilde{k}_1(y - x) + \tilde{b}(\dot{y} - \dot{x}) + k_a(y - z) = d, \tag{12}$$

$$m_1\ddot{x} + \tilde{k}_1(x - y) + \tilde{b}(\dot{x} - \dot{y}) = k_a(y - z), \tag{13}$$

$$m_a\ddot{z} + k_a(z - y) = 0, \tag{14}$$

where $\tilde{k}_1 = k_1 - \hat{k}_1$ and $\tilde{b} = b_a + b$.

Eqs. (12)–(14) turn out to be the governing equations of the system shown in Fig. 4. It is seen that besides the reaction mass, a mass–spring pair $(m_a - k_a)$ of characteristic frequency ω_0 (Eq. (8)) are added to the system. The stiffness k_1 of the original spring is modified to $\tilde{k}_1$, and the damping coefficient of the dashpot is changed to $\tilde{b}$. These pseudo-mechanical elements are emulated by the linear motor via the feedback law of Eqs. (4) and (5); they are hence called *virtual* passive elements. The $m_a - k_a$ pair acts as an ideal vibration absorber for a disturbance of frequency ω_0, as long as the system is stable. The virtual dashpot provides

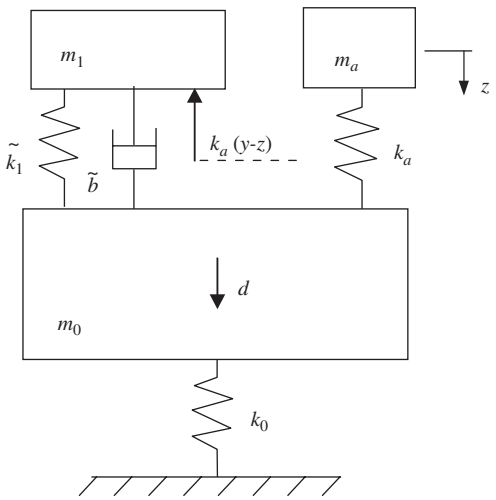

Fig. 4. A mechanical structure equivalent to the closed-loop system of Eqs. (12)–(14).

necessary damping to stabilize the system. Note also the presence of the state-dependent force, $k_a(y-z)$, on the reaction mass. This interaction between the virtual mass and the reaction mass imposes a constraint on the maximum allowable value of m_a, as will be investigated later.

The transfer function from the disturbance to the displacement of the primary body is derived to be

$$\frac{Y(s)}{D(s)} = \frac{(m_1 s^2 + \tilde{b}s + \tilde{k}_1)(m_a s^2 + k_a)}{a_0 s^6 + a_1 s^5 + a_2 s^4 + a_3 s^3 + a_4 s^2 + a_5 s + a_6}, \tag{15}$$

where

$$a_0 = m_0 m_1 m_a, \tag{16}$$
$$a_1 = \tilde{b} m_a (m_0 + m_1), \tag{17}$$
$$a_2 = m_1 m_a (k_0 + k_a + \tilde{k}_1) + m_0 (m_1 k_a + m_a \tilde{k}_1), \tag{18}$$
$$a_3 = \tilde{b}(k_a (m_0 + m_1) + k_0 m_a), \tag{19}$$
$$a_4 = k_a m_1 (k_0 + \tilde{k}_1) + \tilde{k}_1 (m_0 k_a + k_0 m_a), \tag{20}$$
$$a_5 = \tilde{b} k_0 k_a, \tag{21}$$
$$a_6 = k_0 \tilde{k}_1 k_a. \tag{22}$$

Note the existence of a pair of zeros at $\pm i\omega_0$ in Eq. (15). The zeros are independent of the parameters of the passive elements. This verifies that a harmonic disturbance of this frequency will be blocked out in steady state if the system is stable.

4. Stability criteria

To reduce the number of variables in the stability analysis, a set of dimensionless (or normalized) variables are defined

$$m_a^* = m_a/m_0,$$
$$m_1^* = m_1/m_0,$$
$$k_a^* = k_a/k_0.$$

The stability criterion is stated as follows.

Theorem 1. *The closed-loop system of Eqs.* (1)–(6), *given the constraint of Eq.* (7), *is stable if and only if*

$$m_a^* < \frac{m_1^* k_a^* (1 + m_1^*)}{k_a^* + (1 + k_a^*) m_1^*}. \tag{23}$$

Proof. The proof will be conducted using Routh Stability Criteria. The Routh array from Eqs. (15)–(22) is established as follows:

$$\begin{aligned}
&r_{11}(= a_0), \quad r_{12}(= a_2), \quad r_{13}(= a_4), \quad r_{14}(= a_6),\\
&r_{21}(= a_1), \quad r_{22}(= a_3), \quad r_{23}(= a_5),\\
&r_{31}(= a_1 a_2 - a_0 a_3), \quad r_{32}(= a_1 a_4 - a_0 a_5), \quad r_{33}(= a_1 a_6),\\
&r_{41}(= r_{31} a_3 - a_1 r_{32}), \quad r_{42}(= r_{31} a_5 - a_1 r_{33}),\\
&r_{51}(= r_{41} r_{32} - r_{31} r_{42}), \quad r_{52}(= r_{41} r_{33}),\\
&r_{61}(= r_{51} r_{42} - r_{41} r_{52}).
\end{aligned} \tag{24}$$

The terms r_{11} and r_{21} in the Routh array are always positive. The remaining terms of the first column are computed and arranged to be

$$
\begin{aligned}
r_{31} &= \tilde{b}(\tilde{k}_1 m_0^2 + (k_a + 2\tilde{k}_1)m_0 m_1 + (k_0 + k_a + \tilde{k}_1)m_1^2)m_a^2,\\
r_{41} &= \tilde{b}^2 m_a^2 m_1 (k_a^2 m_0^2 + k_0 k_a m_0 m_a + (2k_a^2 m_0 + (k_0^2 + k_0 k_a)m_a)m_1 + k_a^2 m_1^2),\\
r_{51} &= c_1 + c_2\delta,\\
r_{61} &= c_3\delta,
\end{aligned}
$$

where c_1, c_2, c_3 are positive as detailed below.

$$c_1 = c_{11}(c_{12} + c_{13}),$$

where

$$
\begin{aligned}
c_{11} &= \tilde{k}_1 \tilde{b}^3 m_a^3 m_1 (m_0 + m_1),\\
c_{12} &= k_a^3 m_0^3 + k_0 k_a^2 m_0^2 m_a + k_0^2 k_a m_0 m_a^2,\\
c_{13} &= (3k_a^3 m_0^2 + 2k_0 k_a^2 m_0 m_a + (k_0^3 + k_0^2 k_a)m_a^2)m_1 + (3k_a^3 m_0 + k_0 k_a^2 m_a)m_1^2 + k_a^3 m_1^3.
\end{aligned}
$$

Moreover,

$$
\begin{aligned}
c_2 &= \tilde{b}^3 m_a^3 k_0 m_1^2 (m_0 + m_1)k_a^2,\\
c_3 &= (m_0 + m_1)(\tilde{k}_1 m_0^2 + (k_a + 2\tilde{k}_1)m_0 m_1 + (k_0 + k_a + \tilde{k}_1)m_1^2)k_0^2 m_1^2 k_a^3 \tilde{b}^5 m_a^5
\end{aligned}
$$

and

$$\delta = -k_a m_0 m_a + (k_a m_0 + (-k_0 - k_a)m_a)m_1 + k_a m_1^2. \tag{25}$$

It is seen that r_{31} and r_{41} are positive regardless of the magnitudes of the parameters. Stability therefore depends on the signs of r_{51} and r_{61}. Since c_1, c_2, and c_3 are positive, it follows that both $r_{51} > 0$ and $r_{61} > 0$ if and only if $\delta > 0$. From Eq. (25) we have

$$m_a < \frac{k_a m_0 m_1 + k_a m_1^2}{k_a m_0 + (k_0 + k_a)m_1}. \tag{26}$$

Eq. (23) is directly from Eq. (26) using the normalized variables. □

Note that the key step in the proof is to separate r_{51} into two groups: The first group (c_1) involves $\tilde{k}_1$ and is always positive. The second group is factored to get δ. It turns out that r_{61} also contains the factor of δ. Manipulation of the lengthy and tedious algebra is helped by a symbolic mathematics program JACAL, which is a free software and is similar to Maple or the symbolic math toolbox of Matlab.

It is interesting to note from the stability criterion that the system stability is independent of the magnitudes of $\tilde{k}_1$ and $\tilde{b}$, as long as they are positive. By rearranging terms the criterion can be expressed to be

$$m_a^* < m_1^* \frac{k_a^*(1 + m_1^*)}{k_a^*(1 + m_1^*) + m_1^*}. \tag{27}$$

Eq. (27) shows that m_a^* must be smaller than m_1^* for all k_a^*. In other words, for the system to be stable it is required that the virtual mass be *lighter* than the real reaction mass. If k_a^* is much larger than 1, the allowable upper bound for m_a^* tends to m_1^*. The maximum allowable values for m_a^* versus k_a^* are plotted and shown in Fig. 5 for a set of m_1^*.

Note that the above analyses have been based on an undamped primary structure. The stability condition will be much more complicated and may not have a closed form if the structural damping is taken into account. Since passive damping has a stabilizing effect, however, the stability criterion obtained above is

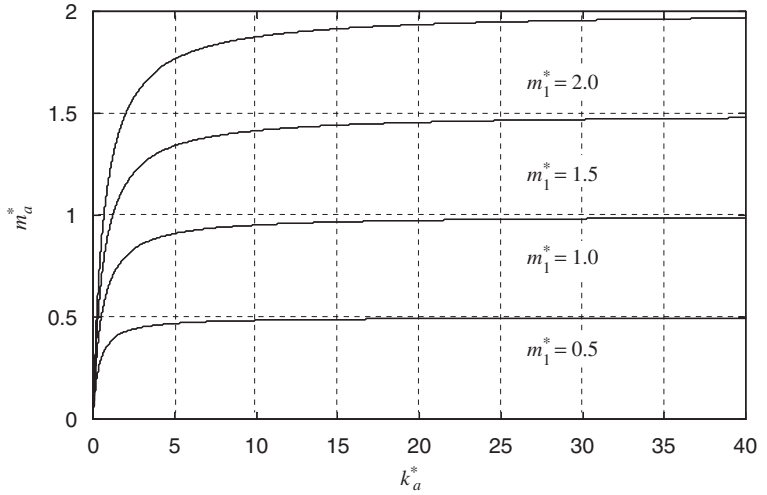

Fig. 5. Maximum allowable m_a^* versus k_a^*. Note that the virtual mass must be *lighter* than the reaction mass.

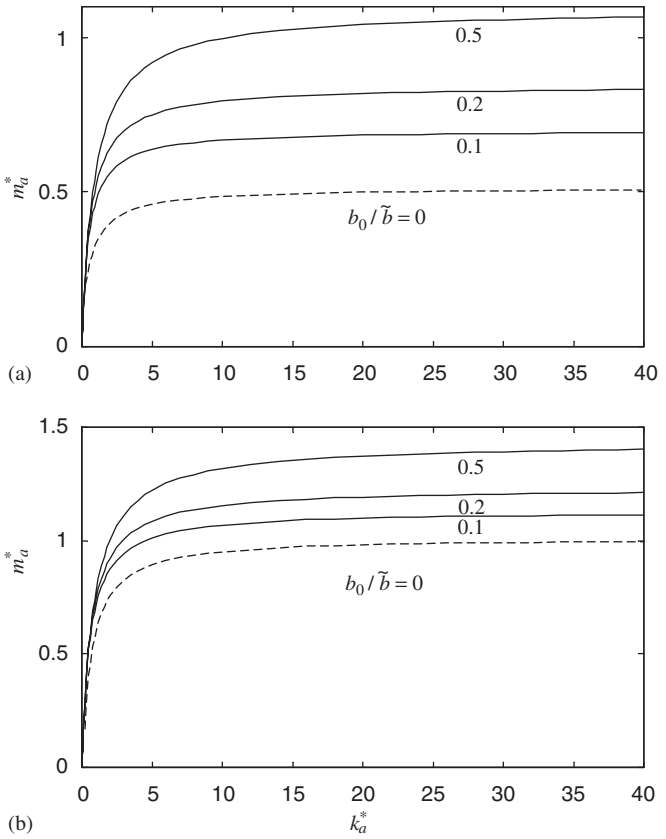

Fig. 6. Stability boundary curves for $b_0/\tilde{b}$ varying from 0 to 0.5: (a) $m_1^* = 0.5$; (b) $m_1^* = 1$.

expected to relax if a damper is added between the primary body and the ground, i.e., if Eq. (1) is modified with an additional damping term to be

$$m_0\ddot{y} + k_0 y + k_1(y - x) + b(\dot{y} - \dot{x}) + b_0\dot{y} = u + d, \tag{28}$$

where b_0 is the damping coefficient of the additional damper. Fig. 6 shows the stability criteria for $b_0/\tilde{b}$ varying from 0 to 0.5, given $\tilde{k}_1/k_0 = 1$, $\tilde{b}/\sqrt{\tilde{k}_1 m_1} = 0.5$. The curves are obtained as follows:

1. Set $k_a = 0$.
2. Repeatedly calculate the poles of the closed-loop system with a gradual increment of m_a from 0 until the first unstable pole is encountered; register the corresponding value of m_a.
3. Increase k_a, and repeat step 2.

Note that unlike the situations with $b_0 = 0$, the stability boundary curve corresponding to a positive $b_0/\tilde{b}$ differs for a different combination of $\tilde{k}_1/k_0$ and $\tilde{b}/\sqrt{\tilde{k}_1 m_1}$, two dimensionless groups. However, extensive numerical calculations indicate the same tendency as shown in Fig. 6. That is, the allowable range for k_a and m_a is enlarged as b_0 is increased from 0. The simple stability criterion of Eq. (27) may therefore serve as a sufficient (but not necessary) stability condition in the practical situations where structural damping is present.

5. Control efforts and transient performance

As mentioned earlier, the mechanical spring k_1 is intended to share the counter-disturbance effort with the linear actuator. Following is an analysis on the distribution of the counter-disturbance force between the passive and the active elements.

Control efforts in steady state: Since y and its time derivatives tend to zero, the terms y and $\ddot{y}$ in Eqs. (1) and (2) vanish in steady state. From Eq. (2), in steady state we have

$$u = -(m_1\ddot{x} + k_1 x + b\dot{x}). \tag{29}$$

Summing up Eqs. (1) and (2) yields

$$d = -m_1\ddot{x}. \tag{30}$$

Let $|u/d|$ represent the *amplitude ratio* of the active control effort to the disturbance in steady state. Since x is a sinusoidal function of frequency ω_0 in steady state, we obtain from Eqs. (29)

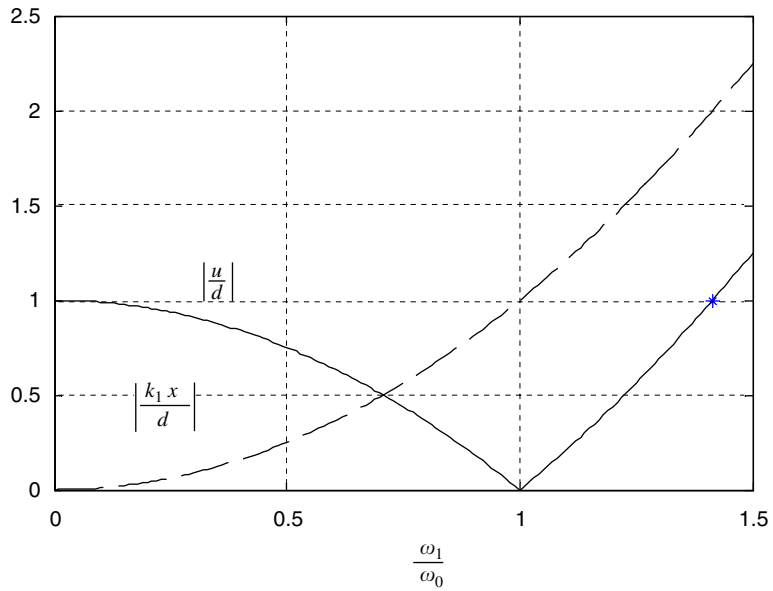

Fig. 7. Active control effort (solid line) and passive spring force (dashed line) in steady state, neglecting the passive damper ($\zeta = 0$).

and (30) that

$$\left|\frac{u}{d}\right| = \frac{\sqrt{(-m_1\omega_0^2 + k_1)^2 + b^2\omega_0^2}}{m_1\omega_0^2}. \tag{31}$$

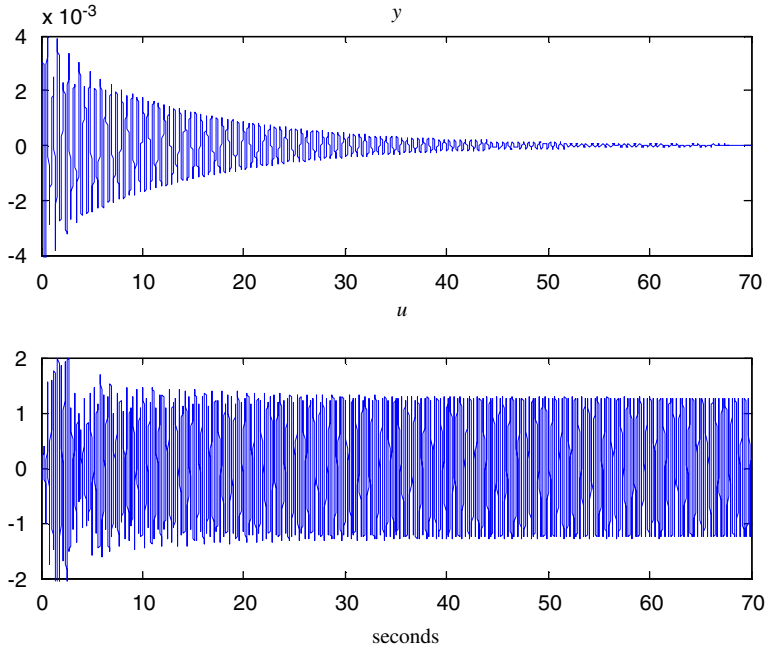

Fig. 8. Simulation results—time response for $\tilde{k}_1 = 1150$.

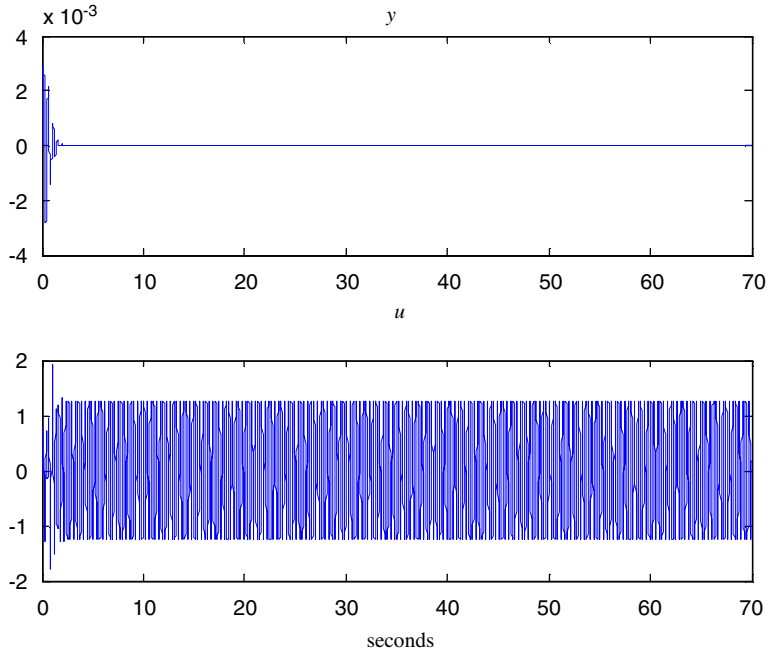

Fig. 9. Simulation results—time response for $\tilde{k}_1 = 200$.

Denote $\omega_1 = \sqrt{k_1/m_1}$ and $\zeta = (1/2)b/\sqrt{k_1 m_1}$, the damping ratio of the passive absorber. Eq. (31) can be written to be

$$\left|\frac{u}{d}\right| = \sqrt{\left(1 - \frac{\omega_1^2}{\omega_0^2}\right)^2 + 4\zeta^2 \frac{\omega_1^2}{\omega_0^2}}. \tag{32}$$

Similarly, the amplitude ratio of the passive spring force to the disturbance can be expressed to be

$$\left|\frac{k_1 x}{d}\right| = \frac{\omega_1^2}{\omega_0^2}. \tag{33}$$

Fig. 7 shows the curves of $|u/d|$ and $|k_1 x/d|$ versus ω_1/ω_0 for $\zeta = 0$. It is seen that if the natural frequency of the $k_1 - m_1$ pair coincides with that of the disturbance, i.e., $\omega_1 = \omega_0$, the control effort from the active device vanishes in steady state. Note, however, in this particular situation the active device is still useful because it helps stabilize the system by adding virtual damping (b_a) to the system without compromising the steady-state performance. As ω_1 deviates away from ω_0, the proportion of the control effort increases. The magnitude of u is equal to that of d if $\omega_1 = \sqrt{2}\omega_0$. Beyond this point the control effort exceeds the disturbance. In other words, if the passive spring is too stiff it is not a help but a "burden" to the active device.

Transient performance: The steady-state response is independent of $\hat{k}_1$, which adjusts the effective stiffness between the reaction mass and the primary body. The value of $\tilde{k}_1$ ($= k_1 - \hat{k}_1$), however, has a significant effect on the transient performance. Figs. 8 and 9 compare the responses of the closed-loop system with different $\hat{k}_1$ by computer simulations. In the simulations, the frequency of disturbance is 3.1 Hz ($\omega_0 = 19.48$ rad/s). The parameters of the system are: $m_0 = 0.6$ kg, $k_0 = 296$ N/m, $m_1 = 1.34$ kg, $k_1 = 1150$ N/m, $b = 0$. The controller's parameters are: $m_a = 0.5$, $k_a = 189.74$, $b_a = 18$ for both simulations. These parameters are chosen to be consistent with the real-time experiments presented later. In Fig. 8, $\hat{k}_1$ is set to be 0 ($\tilde{k}_1 = 1150$), while in Fig. 9 it is set to be 950 so that $\tilde{k}_1$ is reduced to 200. It is seen that the case with smaller $\tilde{k}_1$ has much faster response. Also note that in steady state both cases have the same control efforts regardless of the different $\hat{k}_1$.

Fig. 10 compares the frequency responses for stiff and soft $\tilde{k}_1$. It is seen that there is a significant resonant point (peak) for the case with a stiff effective spring. This can be explained physically by the fact that the stiff spring results in smaller damping ratio: The damping effect diminishes if the spring in parallel to the dashpot is too stiff. Since the value of k_1 is chosen to minimize the steady-state active control effort, one may use $\hat{k}_1$ to adjust the effective stiffness for better transient performance.

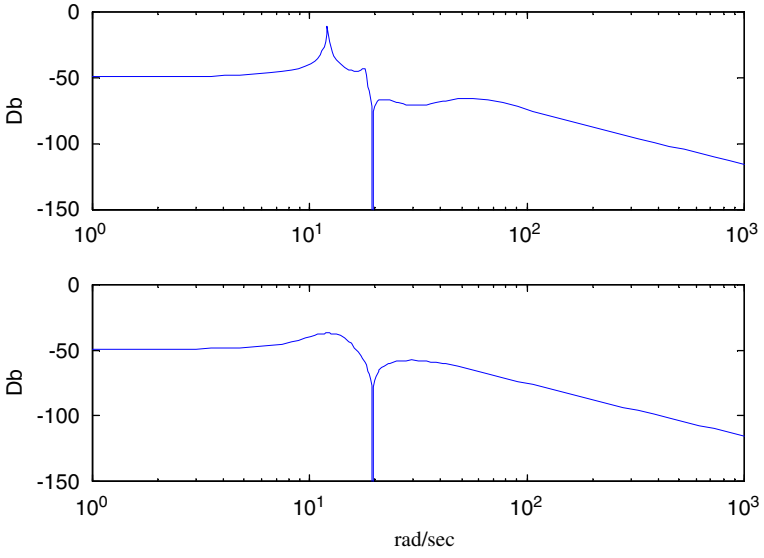

Fig. 10. Frequency responses for different $\tilde{k}_1$: $\tilde{k}_1 = 1150$ (up) and $\tilde{k}_1 = 200$ (down).

Design issues: Considerations in choosing k_1 and $\hat{k}_1$ are given above. Factors in the determination of m_a (and consequently k_a) will be discussed in the following. In general, larger m_a yields faster transient response since k_a increases with m_a for a given ω_0 ($k_a = m_a\omega_0^2$), and larger k_a in turn means higher gain in the feedback algorithm. However, besides the constraint of the power available from the linear actuator, stability must be taken into account in determining the size of the virtual mass. In the above simulation, $k_a^* = 189.74/296 = 0.641, m_1^* = 1.34/0.6 = 2.23$, and $m_a^* = 0.5/0.6 = 0.833$, which is below the critical value dictated by Eq. (23): $2.23 \times 0.641 \times (1 + 2.23)/(0.641 + (1 + 0.641) \times 2.23) = 1.074$. Stability is therefore ensured for the closed-loop system. This example shows that parameters of the primary structure can be uncertain to an extent but their bounds must be known, so that stability condition can be checked. Numerical simulations on the nominal system are also helpful in fine-tuning the controller's parameters before real-time implementation.

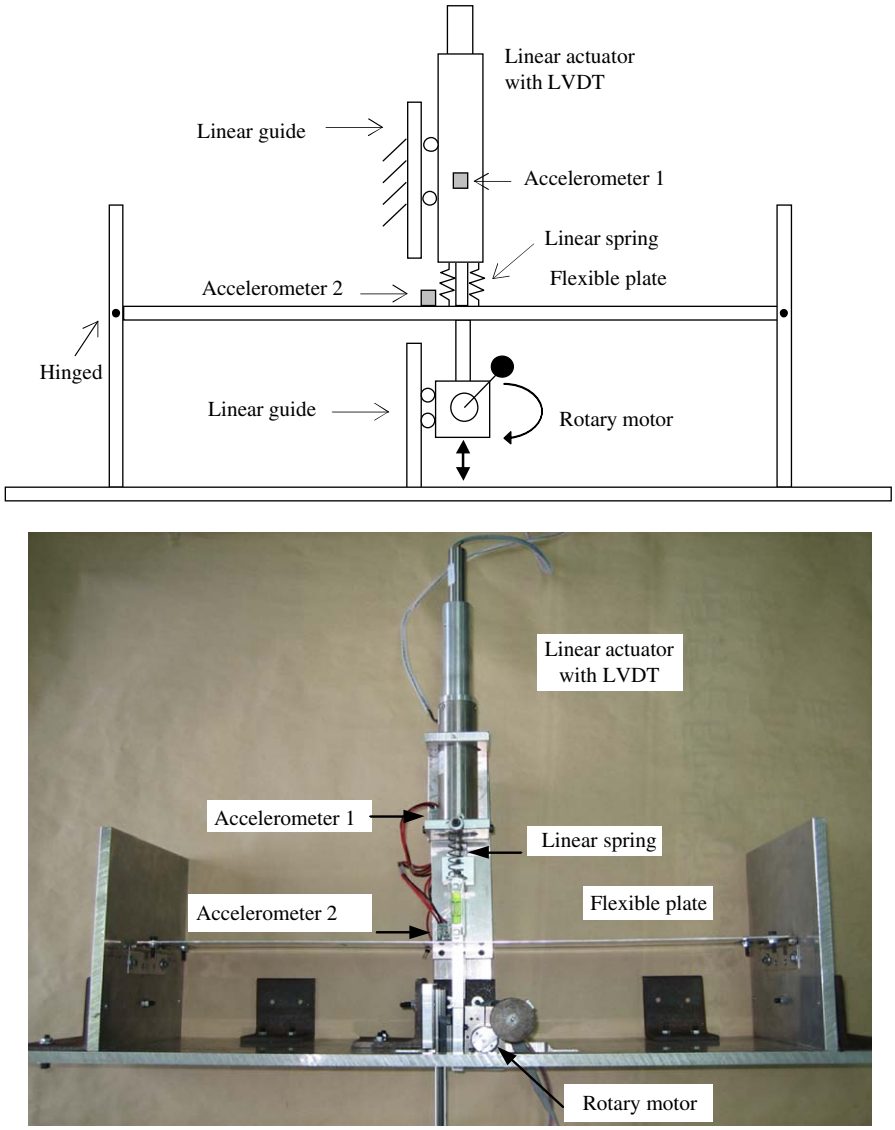

Fig. 11. Experimental apparatus: the functional sketch (up) and the photo (down). Accelerometer 2 is installed to evaluate the response of the flexible plate.

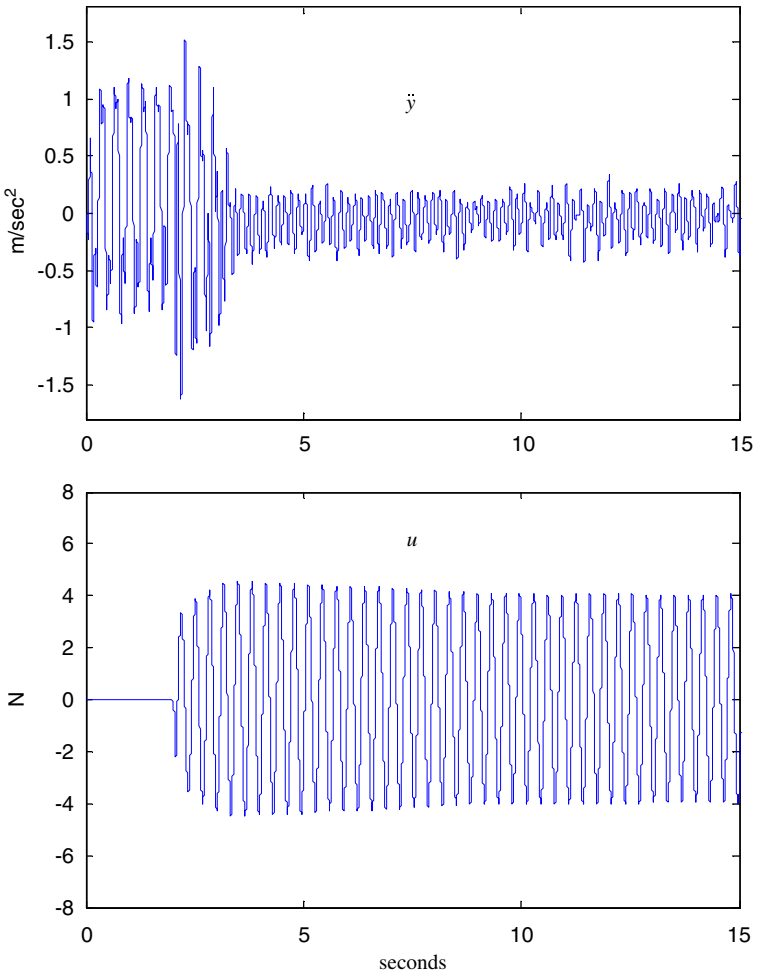

Fig. 12. Experimental results; the controller is activated after 2 s.

6. Experimental results

Fig. 11 shows the picture of the experimental system for real-time testing. The flexible plate is hinged at both ends. A rotary motor with an eccentric load is attached to the center of the flexible plate. It is set to rotate at a constant speed (3.1 revolutions/s), imposing a harmonic disturbance to the plate. The linear actuator is a moving-magnet voice-coil motor; its shaft is attached to the flexible plate and its body is connected to the plate via a mechanical spring (k_1). An accelerometer is glued to the body of the actuator for the feedback controller. Another accelerometer is glued to the center of the flexible plate to monitor vibrations before and after control activation. The flexible plate is modeled as a mass–spring structure ($m_0 - k_0$) and the body of the linear actuator functions as the reaction mass (m_1). Parameters of the system are as given in the previous section.

Fig. 12 shows the time response of the closed-loop system under a discrete version of Eqs. (4) and (5). The parameters of the controller are as follows: $m_a = 0.5$, $k_a = 189.74$, $b = 18$, and $\hat{k}_1 = 0$. The controller is activated after 2 s. It is seen that oscillations are significantly reduced by the control action. The transient time is much shorter than in the simulation result of Fig. 8. This can be explained by the presence of structural damping and friction in the flexible plate, which are not included in the simulation model. Unlike the simulation, however, there are some residual vibrations in steady state. These oscillations can be attributed to the high-frequency harmonics excited by the rotary motor, as analyzed below.

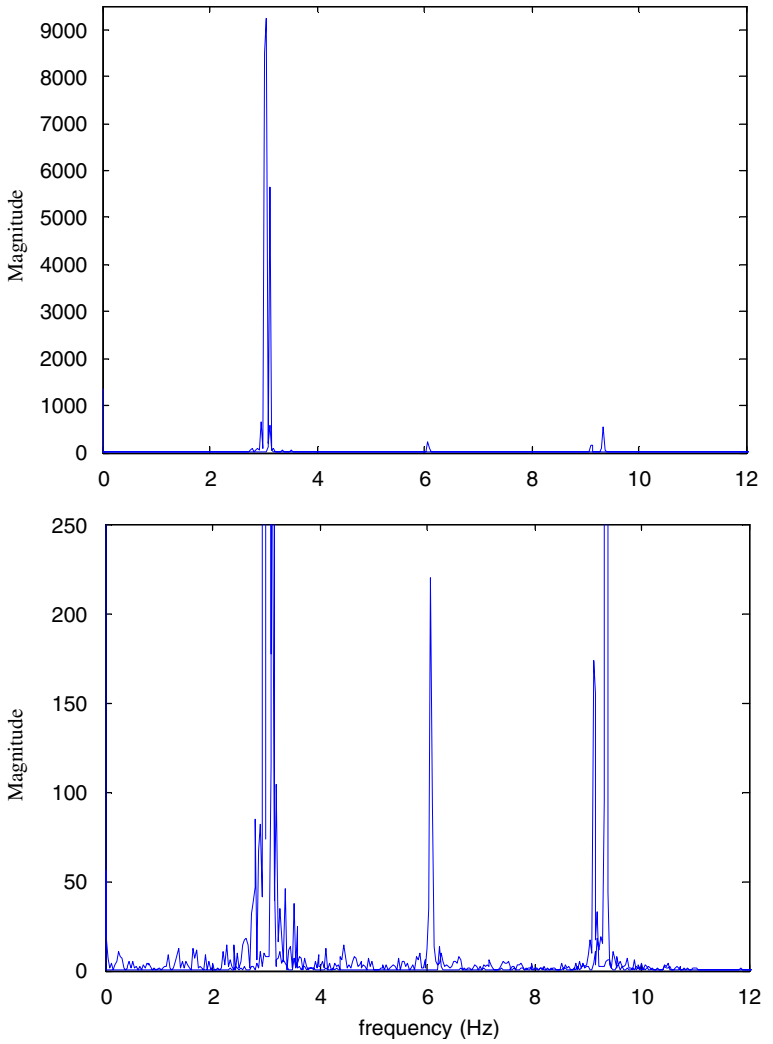

Fig. 13. Spectrum of $\ddot{y}$ without control (up) and the amplified picture (down). Note the presence of higher harmonics.

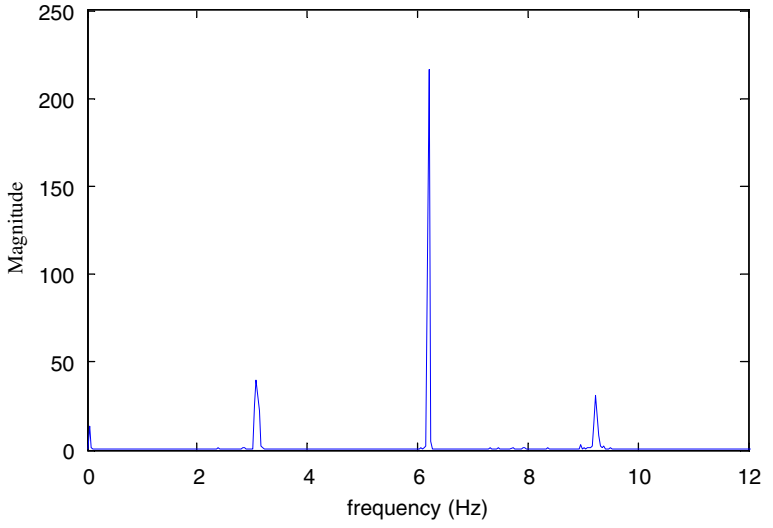

Fig. 14. Spectrum of $\ddot{y}$ with control. The second harmonic remains.

Figs. 13 and 14 compare the spectrum of the accelerations at the midsection of the flexible plate before and after control, obtained by a fast Fourier transform (FFT) routine on the time-response data. It is seen that the component at 3.1 Hz is drastically reduced. The residual oscillations are mostly due to the second harmonic (6.2 Hz). This is consistent with the fact that the active absorber is targeted at 3.1 Hz.

7. Conclusions

A hybrid DVA representable by an equivalent mechanical structure with a state-dependent force is developed. A simple, closed-form stability criterion is derived. Stability is ensured if the value of the virtual mass (m_a^*) lies below an upper bound depending on m_1^* and k_a^*. The hybrid DVA is capable of neutralizing the harmonic disturbance regardless of the detailed parameters of the passive elements, although the bounds on the inertia and stiffness of the primary structure must be available for checking the stability condition in advance. Distribution of the counter-disturbance force between the passive and active devices is also analyzed. Both numerical simulations and real-time experiments confirm the effectiveness of the proposed method.

Acknowldgments

This research is supported by the National Science Council, Taiwan, ROC, under Grant number NSC93-2218-E-2214-005.

References

[1] J.Q. Sun, M.R. Jolly, M.A. Norris, Passive, adaptive and active tuned vibration absorbers—a survey, *ASME Journal of Dynamic Systems, Measurement and Control* 117 (1995) 234–242.
[2] N. Olgac, B. Holm-Hansen, A novel active vibration absorption technique: delayed resonator, *Journal of Sound and Vibration* 176 (1994) 93–104.
[3] H. Elmali, M. Renzulli, N. Olgac, Experimental comparison of delayed resonator and PD controlled vibration absorbers using electromagnetic actuators, *ASME Journal of Dynamic Systems, Measurement, and Control* 122 (2000) 514–520.
[4] J. Yuan, Hybrid dynamic vibration absorption by zero/pole placement, *ASME Journal of Vibration and Acoustics* 122 (2000) 466–469.
[5] D. Filipovi, D. Schroder, Bandpass vibration absorber, *Journal of Sound and Vibration* 214 (3) (1998) 553–566.
[6] Y.-D. Chen, C.-C. Fuh, P.-C. Tung, Application of voice coil motors in active dynamic vibration absorbers, *IEEE Transactions on Magnetics* 41 (3) (2005) 1149–1154.
[7] M. Yasuda, R. Gu, O. Nishihara, H. Matsuhisa, K. Ukai, M. Kondo, Development of anti-resonance enforced active vibration absorber system, *JSME International Journal Series C* 39 (3) (1996) 464–469.
[8] G.A. Lesieutre, R. Rusovici, G.H. Koopmann, J.J. Dosch, Modeling and characterization of a piezoceramic inertial actuator, *Journal of Sound and Vibration* 261 (1) (2003) 93–107.
[9] Y. Zhang, A. Alleyne, A simple novel approach to active vibration isolation with electrohydraulic actuation, *Journal of Dynamic Systems, Measurement, and Control* 125 (2003) 125–128.
[10] R.A. Burdisso, J.D. Heilmann, A new dual-reaction mass dynamic vibration absorber actuator for active vibration control, *Journal of Sound and Vibration* 214 (5) (1998) 817–831.
[11] T. Tantanawat, Z. Li, S. Kota, Application of compliant mechanisms to active vibration isolation systems, *Proceedings of DETC 2004*, *International Design Engineering Technical Conference*, Salt Lake City, Utah, September 28–October 2, 2004.
[12] Y. Du, R.A. Burdisso, E. Nikolaidis, Control of internal resonances in vibration isolators using passive and hybrid dynamic vibration absorbers, *Journal of Sound and Vibration* 286 (2005) 697–727.
[13] S.-J. Huang, W.-C. Lin, Adaptive fuzzy controller with sliding surface for vehicle suspension control, *IEEE Transactions on Fuzzy Systems* 11 (4) (2003) 550–559.
[14] S.-T. Wu, Virtual vibration absorbers with inherent damping, *AIAA Journal of Guidance, Dynamics, and Control* 25 (4) (2002) 644–650.
[15] S.-T. Wu, Y.-C. Chuang, Output regulation of robot manipulators with a constantly revolving arm, *IEEE Transactions on Robotics and Automation* 19 (6) (2003) 1002–1006.